

## A LATE-TIME FLATTENING OF LIGHT CURVES IN GAMMA-RAY BURST AFTERGLOWS

LORENZO SIRONI<sup>1,3</sup> AND DIMITRIOS GIANNIOS<sup>2</sup>

<sup>1</sup>Harvard-Smithsonian Center for Astrophysics, 60 Garden Street, Cambridge, MA 02138, USA

<sup>2</sup>Department of Physics, Purdue University, 525 Northwestern Avenue, West Lafayette, IN 47907, USA

<sup>3</sup>NASA Einstein Postdoctoral Fellow

*Draft version September 11, 2018*

### ABSTRACT

The afterglow emission from Gamma-Ray Bursts (GRBs) is usually interpreted as synchrotron radiation from relativistic electrons accelerated at the GRB external shock, that decelerates from ultra-relativistic to non-relativistic speeds as it sweeps up the surrounding medium. We investigate the temporal decay of the emission from GRB afterglows at late times, when the bulk of the shock-accelerated electrons are non-relativistic. For a uniform circumburst medium, we show that such “deep Newtonian phase” begins at  $t_{\text{DN}} \sim 3 \epsilon_{e,-1}^{5/6} t_{\text{ST}}$ , where  $t_{\text{ST}}$  marks the transition of the blast wave to the non-relativistic spherically-symmetric Sedov–Taylor solution, and  $\epsilon_e = 0.1 \epsilon_{e,-1}$  quantifies the amount of shock energy transferred to the post-shock electrons. For typical parameters, the deep Newtonian stage starts  $\sim 0.5$ –several years after the GRB. The radio flux in this phase decays as  $F_\nu \propto t^{-3(p+1)/10} \propto t^{-(0.9 \div 1.2)}$ , for a power-law distribution of shock-accelerated electrons with slope  $2 < p < 3$ . This is shallower than the commonly assumed scaling  $F_\nu \propto t^{-3(5p-7)/10} \propto t^{-(0.9 \div 2.4)}$  derived by Frail et al. (2000), which only applies if the GRB shock is non-relativistic, but the electron distribution still peaks at ultra-relativistic energies (a regime that is relevant for a narrow time interval, and only if  $t_{\text{DN}} \gtrsim t_{\text{ST}}$ , or  $\epsilon_e \gtrsim 0.03$ ). We discuss how the deep Newtonian phase can be reliably used for GRB calorimetry, and we comment on the good detection prospects of trans-relativistic blast waves at  $0.1 \div 10$  GHz with EVLA and LOFAR.

*Subject headings:* gamma-ray burst: general — radiation mechanisms: non-thermal — shock waves

### 1. INTRODUCTION

Afterglow radiation from Gamma-Ray Bursts (GRBs) is attributed to external shocks produced by the interaction between the ultra-relativistic ejecta and the circumburst medium. Synchrotron emission from the shock-accelerated electrons powers the observed afterglow, detected in the  $\gamma$ -ray, X-ray, optical and radio bands (e.g., Sari et al. 1998; Wijers & Galama 1999; Panaitescu & Kumar 2000; Granot & Sari 2002; Kumar & Barniol Duran 2009). Nowadays, GRB afterglows are observed at times as early as the prompt emission at X-ray and optical frequencies, and up to a few years after the GRB at radio wavelengths.

As the blast wave sweeps up the surrounding medium, the external shock slows down to non-relativistic velocities, and it finally approaches spherical symmetry (e.g., Sari et al. 1998, 1999; Rhoads 1999; Livio & Waxman 2000; Zhang & MacFadyen 2009). At this point, the dynamics can be described by the non-relativistic spherically-symmetric Sedov–Taylor (ST) solution. The radiation from the external shock can be calculated by assuming synchrotron emitting electrons with a power-law energy spectrum  $dN/d\gamma \propto \gamma^{-p}$ , for  $\gamma \geq \gamma_m$ .<sup>1</sup> The minimum Lorentz factor  $\gamma_m$  is related to the fraction  $\epsilon_e$  of shock energy transferred to the accelerated electrons by  $\gamma_m - 1 = \frac{p-2}{p-1} \epsilon_e (\Gamma - 1) m_p / m_e$ , where  $\Gamma$  is the bulk

Lorentz factor of the blast wave. By assuming  $\gamma_m \gg 1$ , Frail et al. (2000) found that the synchrotron flux in the radio band should decay as  $F_\nu \propto t^{-3(5p-7)/10}$ , after the shock becomes non-relativistic (i.e.,  $\Gamma - 1 \ll 1$ ).

The assumption that the low-energy end of the electron distribution stays ultra-relativistic breaks down as soon as  $\Gamma - 1 \lesssim \epsilon_e^{-1} m_e / m_p$ . When the peak of the electron distribution drops down to non-relativistic energies, the system will transition to a new regime, which we shall call the “deep Newtonian phase.” In the deep Newtonian stage, the theory of diffusive shock acceleration predicts that, while most of the shock-heated electrons are non-relativistic, the bulk of the electron energy is contributed by mildly relativistic particles with  $\gamma_{\text{pk}} \sim 2$  (e.g., Bell 1978; Blandford & Ostriker 1978; Blandford & Eichler 1987). This is opposite to the case typically considered in relativistic shocks, where for  $\gamma_m \gg 1$  and  $p > 2$  the particles with  $\gamma_{\text{pk}} \sim \gamma_m$  dominate *both* the number and the energy census (Sari et al. 1998).

In this work, we study the synchrotron light curves expected in the deep Newtonian regime. As we show in Section 2, we find that this phase begins at  $t_{\text{DN}} \sim 3 \epsilon_{e,-1}^{5/6} t_{\text{ST}}$ , where  $t_{\text{ST}}$  marks the transition of the blast wave to the non-relativistic spherically-symmetric ST solution, and  $\epsilon_e = 0.1 \epsilon_{e,-1}$ . For  $2 < p < 3$ , we find that the radio flux decays as  $F_\nu \propto t^{-3(p+1)/10} \propto t^{-(0.9 \div 1.2)}$ , which is shallower than the regime discussed by Frail et al. (2000), and nearly independent of the uncertain power-law slope  $p$ . The GRB afterglows with the longest follow-ups (e.g., GRB 030329, still visible in radio waves years after the explosion) are likely to be in the deep Newtonian phase, so our results can be used to perform reliable calorimet-

Email: lsironi@cfa.harvard.edu; dgiannio@purdue.edu.

<sup>1</sup> For the sake of simplicity, in the following we assume that all of the post-shock electrons are contained in the power-law tail (i.e., the number fraction of shock-accelerated electrons is  $\zeta_e = 1$ ). Also, throughout the text we reserve the lower case  $\gamma$  for the random particle Lorentz factor and upper case  $\Gamma$  for the fluid bulk motion.

ric estimates of the explosions. Although our main focus is on GRB afterglows, our results can be equally applied to radio afterglows from tidal disruption events, radio supernovae, and trans-relativistic ejecta from neutron star mergers, as we discuss in Section 3. Finally, we summarize our findings in Section 4, where we also comment on the detection prospects of late afterglows at 0.1–10 GHz with EVLA and LOFAR.

## 2. THE NON-RELATIVISTIC AFTERGLOW STAGES

### 2.1. Analytical Estimates

In this section we use analytical arguments to calculate the GRB light curve in the non-relativistic stages, and its dependence on the various model parameters of the GRB blast wave. Our analytical estimates are verified and calibrated by the numerical results of Section 2.2.

Let us consider a jet with (beaming-corrected) energy  $E_j = 10^{51.5} E_{51.5}$  erg propagating in a uniform medium<sup>2</sup> with number density  $n = 10 n_1 \text{ cm}^{-3}$ . According to the analytical study by Wygoda et al. (2011) and the relativistic hydrodynamic simulations by van Eerten & MacFadyen (2012), the spherical ST solution can be used to estimate the observed flux for on-axis observers at a time

$$t \gtrsim t_{\text{ST}} \simeq 200 (E_{51.5}/n_1)^{1/3} \text{ days}, \quad (1)$$

which typically follows the deceleration of the blast wave down to non-relativistic speeds (Piran 2004; Zhang & MacFadyen 2009).<sup>3</sup> After the transition to the ST solution, the blast wave radius evolves in time as

$$R \simeq 7.5 \times 10^{17} (E_{51.5}/n_1)^{1/5} t_{\text{yr}}^{2/5} \text{ cm}, \quad (2)$$

and its velocity in units of the speed of light is

$$\beta \simeq 0.3 (E_{51.5}/n_1)^{1/5} t_{\text{yr}}^{-3/5}, \quad (3)$$

where  $t_{\text{yr}}$  is the observer time in years. If the shock-accelerated electrons populate a power law of index  $p$  containing a fraction  $\epsilon_e$  of the shock-dissipated energy, then the minimum electron Lorentz factor will be

$$\gamma_m - 1 \simeq \frac{p-2}{p-1} \epsilon_e \frac{m_p \beta^2}{2 m_e} \equiv \frac{1}{8} \bar{\epsilon}_e \frac{m_p \beta^2}{m_e}, \quad (4)$$

where for compactness we have set  $\bar{\epsilon}_e \equiv \epsilon_e 4(p-2)/(p-1)$ . The “deep Newtonian phase” will start at the time  $t_{\text{DN}}$  when  $(\gamma_m - 1)m_e c^2 \sim m_e c^2$ , i.e., the bulk of the shock-accelerated electrons turn non-relativistic. This gives

$$t_{\text{DN}} \simeq 1.5 (E_{51.5}/n_1)^{1/3} \bar{\epsilon}_e^{-5/6} \text{ years}, \quad (5)$$

where  $\bar{\epsilon}_e = 0.1 \bar{\epsilon}_{e,-1}$ . This estimate for  $t_{\text{DN}}$  is in good agreement with the numerical results of Section 2.2.

We now estimate the synchrotron flux expected in the radio band. Let us parameterize the post-shock magnetic energy density as being a fraction  $\epsilon_B = 0.01 \epsilon_{B,-2}$  of the thermal energy density of the shocked fluid  $e_{th} \sim 2 n m_p \beta^2 c^2$ , so that the field strength is

$$B \simeq 0.04 \epsilon_{B,-2}^{1/2} E_{51.5}^{1/5} n_1^{3/10} t_{\text{yr}}^{-3/5} \text{ G}. \quad (6)$$

<sup>2</sup> In Appendix B we perform a similar analysis, for a wind profile.

<sup>3</sup> In the following, we neglect the effect of the cosmological redshift, since the late afterglow emission is observable only in relatively nearby ( $z \lesssim 0.5$ ) bursts, where redshift corrections are small.

When the low-energy end of the electron distribution is still ultra-relativistic (i.e., in the limit by Frail et al. (2000)), the characteristic synchrotron frequency  $\nu_{\text{pk}} \propto \gamma_{\text{pk}}^2 B$  will be emitted by electrons with  $\gamma_{\text{pk}} \sim \gamma_m$ , so

$$\nu_{\text{pk}} \sim \nu_m \simeq 10^6 \bar{\epsilon}_{e,-1}^2 \epsilon_{B,-2}^{1/2} E_{51.5} n_1^{-1/2} t_{\text{yr}}^{-3} \text{ Hz}. \quad (7)$$

The overall luminosity  $L_{\text{pk}} \sim L_m$  at the peak frequency is the product of the total number of radiating electrons ( $\propto R^3 n$ ) and the peak power of a single electron ( $\propto B$ ). Using the definition of  $\gamma_m$  in Equation (4), we can alternatively write that  $L_{\text{pk}} \propto B R^3 \bar{\epsilon}_e e_{th}/(\gamma_m - 1)$ , an expression that will be useful below. We obtain

$$L_{\text{pk}} \sim L_m \simeq 3 \times 10^{32} \epsilon_{B,-2}^{1/2} E_{51.5}^{4/5} n_1^{7/10} t_{\text{yr}}^{3/5} \text{ erg s}^{-1} \text{ Hz}^{-1} \quad (8)$$

and the flux observed at 1 GHz (for a burst with luminosity distance  $d_L \simeq 10^{27.5} d_{27.5}$  cm, as appropriate for GRB 030329) is

$$F_\nu = L_m / (4\pi d_L^2) (\nu_m/\nu)^{(p-1)/2} \\ \simeq 0.3 \bar{\epsilon}_{e,-1}^{p-1} \epsilon_{B,-2}^{\frac{1+p}{4}} E_{51.5}^{\frac{3+5p}{10}} n_1^{\frac{19-5p}{20}} t_{\text{yr}}^{\frac{3(7-5p)}{10}} \nu_{\text{GHz}}^{\frac{1-p}{2}} d_{27.5}^{-2} \text{ mJy} \quad (9)$$

which has been rescaled down by a factor of  $\sim 4$  to match the numerical results obtained in Section 2.2 at  $t = 1000$  days. The last expression assumes optically thin emission of slow-cooling electrons in the observed band. This is typically the case at  $\gtrsim$  GHz frequencies and years after the burst (we refer to Appendix C for a discussion of the role of synchrotron self-absorption).

#### 2.1.1. The Deep Newtonian Regime

The analysis above applies to the limit discussed by Frail et al. (2000), i.e., the blast wave is non-relativistic, but the distribution of shock-heated electrons has  $\gamma_m \gg 1$ . The applicability of this regime is rather narrow. Independently of the choice of  $\epsilon_e$ , the electrons eventually turn non-relativistic, and the previous afterglow treatment becomes invalid. Moreover, as shown in Equations (1) and (5), in the case  $\bar{\epsilon}_e \lesssim 0.03$  the electrons become non-relativistic before the blast wave relaxes to the ST solution, so the non-relativistic stage discussed by Frail et al. (2000) does not occur.

While in the limit presented by Frail et al. (2000) most of the electron energy is contributed by particles with  $\gamma_{\text{pk}} \sim \gamma_m$ , in the deep Newtonian phase the energy census is dominated by electrons with  $\gamma_{\text{pk}} \sim 2$ . This follows from the theory of Fermi acceleration in shocks (e.g., Blandford & Ostriker 1978; Bell 1978; Blandford & Eichler 1987). The reason is that the spectrum of accelerated particles follows a power-law distribution in *momentum* with slope  $p$ . In units of the dimensionless kinetic energy  $x = \gamma - 1$ , we obtain  $dN/dx \propto (x^2 + 2x)^{-(p+1)/2} (1+x)$ , for  $x \geq \gamma_m - 1$ . For  $\gamma_m \gg 1$ , one recovers the familiar ultra-relativistic result, with the energy census dominated by electrons having  $\gamma_{\text{pk}} \sim \gamma_m$ . In contrast, for  $\gamma_m - 1 \ll 1$  and  $2 < p < 3$ , the energy of the electron distribution (i.e.,  $x^2 dN/dx$ ) peaks at  $x_{\text{pk}} \sim 1$ , or  $\gamma_{\text{pk}} \sim 2$ .<sup>4</sup>

<sup>4</sup> When  $p \geq 3$  our treatment is not applicable since  $\gamma_m$  dominates both in energy and particle number (as in the ultra-relativistic case). Since theory and observations suggest that  $p < 3$ , in the

In the deep Newtonian phase, the flux declines as  $F_\nu \propto t^{-3(1+p)/10}$ , due to the following argument. The peak synchrotron frequency  $\nu_{\text{pk}}$  will be emitted by the electrons contributing most of the energy, i.e., with  $\gamma_{\text{pk}} \sim 2$ . So, the peak frequency in the deep Newtonian phase is

$$\nu_{\text{pk}} \simeq 4 \times 10^5 \epsilon_{\text{B},-2}^{1/2} E_{51.5}^{1/5} n_1^{3/10} t_{\text{yr}}^{-3/5} \text{ Hz}. \quad (10)$$

The luminosity emitted at the peak frequency scales as  $L_{\text{pk}} \propto BR^3 \bar{\epsilon}_e e_{th}/\gamma_{\text{pk}}$ , which is the same expression as before, but with  $\gamma_m$  replaced by  $\gamma_{\text{pk}}$ . We obtain  $L_{\text{pk}} \propto t^{-3/5}$ . So, the flux at the frequency  $\nu$  scales as

$$F_\nu = L_{\text{pk}}/(4\pi d_L^2) (\nu_{\text{pk}}/\nu)^{(p-1)/2} \propto t^{-\frac{3(1+p)}{10}} \nu^{\frac{1-p}{2}} \quad (11)$$

By matching this temporal decay with the flux in Equation (9) computed at the transition time  $t = t_{\text{DN}}$ , we find the flux in the deep Newtonian phase to be

$$F_\nu = 0.2 \bar{\epsilon}_{e,-1} \epsilon_{\text{B},-2}^{\frac{1+p}{4}} E_{51.5}^{\frac{11+p}{10}} n_1^{\frac{3+3p}{20}} t_{\text{yr}}^{\frac{-3(1+p)}{10}} \nu_{\text{GHz}}^{\frac{1-p}{2}} d_{27.5}^{-2} \text{ mJy} \quad (12)$$

The numerical value is calibrated by the simulation results of Section 2.2 at  $t = 1000$  days, for a burst with luminosity distance  $d_L \simeq 10^{27.5}$  cm, as appropriate for GRB 030329. The simulations also verify the dependence of the flux on the various model parameters as predicted by Equation (12).

Finally, we point out that the scalings derived above can be recovered in the formalism appropriate to the ultra-relativistic case  $\gamma_m \gg 1$ , modulo a few changes. When  $\gamma_m$  falls below unity, i.e., at the onset of the deep Newtonian phase, one should set  $\gamma_m = 1$ , and account for the fact that only a small fraction of the electrons are now ultra-relativistic. If the fraction of accelerated electrons is constant and equal to  $\zeta_{e,\text{UR}}$  when  $\gamma_m \gg 1$  (in this work, we assume  $\zeta_{e,\text{UR}} = 1$  for simplicity), during the deep Newtonian phase it is sufficient to replace  $\zeta_{e,\text{UR}}$  by  $\zeta_{e,\text{DN}} = \zeta_{e,\text{UR}} \frac{p-2}{p-1} \epsilon_e (\Gamma - 1) m_p/m_e \ll 1$ , which evolves as  $\zeta_{e,\text{DN}} \propto \beta^2 \propto t^{-6/5}$ .

## 2.2. Synthetic Light Curves from Relativistic Hydrodynamical Simulations

Our analytical estimates are based on a simple model where the blast wave is assumed to relax into a spherical ST solution at its non-relativistic stages. Here we demonstrate that such a model gives a fairly good description of the observed properties of the blast wave, by comparing our analytical estimates to the results of relativistic hydrodynamical simulations.

### 2.2.1. The New Prescription for Particle Acceleration

We have computed synthetic light curves of GRB afterglows in the radio band by employing the *Afterglow Library* described in van Eerten et al. (2012) (see also Zhang & MacFadyen 2009; van Eerten & Wijers 2009; van Eerten et al. 2010a,b; van Eerten & MacFadyen 2011).<sup>5</sup> The library calculates the full light curves and spectra using linear radiative transfer (including synchrotron self-absorption) through snapshots of relativistic hydrodynamical simulations of GRB jets.

main text we only explore the case  $2 < p < 3$ , and we defer to Appendix A the treatment of steeper particle distributions.

<sup>5</sup> The *Afterglow Library* is publicly available at <http://cosmo.nyu.edu/afterglowlibrary>.

The hydrodynamical simulations employed by van Eerten et al. (2012) can follow the GRB jet from the ultra-relativistic phase down to non-relativistic velocities. When computing the radiative signature of GRB afterglows, van Eerten et al. (2012) implicitly assumed that the distribution of emitting electrons is a power law in energy of the form  $dN/d\gamma \propto \gamma^{-p}$  for  $\gamma \geq \gamma_m = \frac{p-2}{p-1} \epsilon_e e_{th,loc}/(n_{loc} m_e c^2)$ , where  $e_{th,loc}$  and  $n_{loc}$  are the thermal energy density and the number density of the local fluid.<sup>6</sup> As we have discussed in Section 2.1, such a parametrization is not appropriate for  $t \gtrsim t_{\text{DN}}$ , when the bulk of the accelerated electrons become non-relativistic (and  $\gamma_m$  as defined above falls below unity).

We have modified the radiation module of the *Afterglow Library* to account for the transition to the deep Newtonian regime. When  $\gamma_m$  (as defined above) falls below unity, we set  $\gamma_m = 1$ .<sup>7</sup> Also, the emission and absorption coefficients are taken to be proportional to  $(p-2)\epsilon_e e_{th,loc}/(\gamma_m m_e c^2)$ , which is valid both for ultra-relativistic electrons [it reduces to  $(p-1)n_{loc}$ , when  $\gamma_m = \frac{p-2}{p-1} \epsilon_e e_{th,loc}/(n_{loc} m_e c^2) \gg 1$ ] and in the deep Newtonian regime (with  $\gamma_m = 1$ ).

In principle, the transition to the Newtonian regime could be accompanied by several other changes in the distribution of accelerated electrons. For example, the power-law slope might decrease from the universal prediction  $p \simeq 2.23$  of Fermi acceleration in relativistic shocks (Kirk et al. 2000; Keshet & Waxman 2005) to the standard value  $p \simeq 2$  expected in non-relativistic shocks (e.g., Blandford & Eichler 1987). Or, the fraction  $\epsilon_e$  of shock energy transferred to the accelerated electrons might drop by one or two orders of magnitude, as the blast wave becomes non-relativistic. However, the magnitude of such changes is still a subject of active research, and we do not implement them in our radiation module. In contrast, the evolution of the bulk electrons down to non-relativistic energies is an *inevitable* outcome of the deceleration of the blast wave at  $t \gtrsim t_{\text{DN}}$ . We now show how this affects the late-time light curves of GRB radio afterglows.

### 2.2.2. Results

In Figure 1, we show GRB light curves at 5 GHz for on-axis observers, computed using the *Afterglow Library* described in van Eerten et al. (2012). We neglect the contribution of the counter-jet, to emphasize how our results differ from the prescription of electron acceleration employed by earlier studies.

In the top panel, we show that the late-time evolution (solid lines) is well described by a power law, with the slope predicted by Equation (12) (dotted lines). The temporal decay in our model (solid lines) is always shallower than in the regime discussed by Frail et al. (2000, dashed lines), in agreement with the analytical estimates in Equation (9) and Equation (12). As the electron power-law slope  $p$  varies from 2 to 3, the difference

<sup>6</sup> So far, we have used  $e_{th}$  for the thermal energy density of the material right behind the shock, whereas  $n$  was the number density of the circumburst medium.

<sup>7</sup> We have tested that a different choice for the threshold value (yet, still of order unity) does not appreciably change the light curves in the deep Newtonian phase.

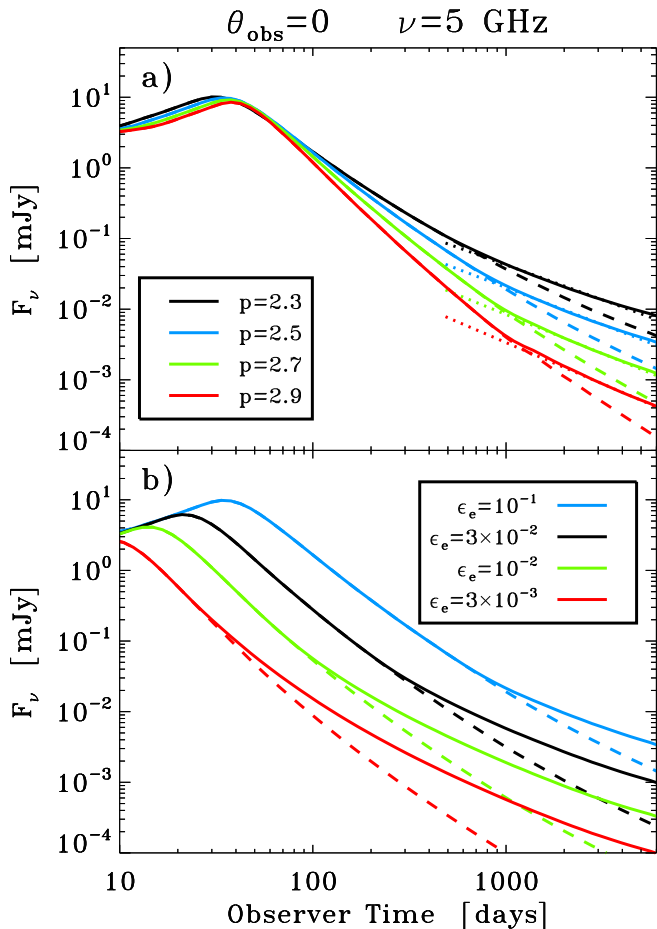


FIG. 1.— Synthetic light curves extracted from relativistic hydrodynamical simulations, for on-axis observers (i.e.,  $\theta_{\text{obs}} = 0$ ) at frequency  $\nu_{\text{obs}} = 5$  GHz. We employ  $E_{51.5} = 1$ ,  $n_1 = 1$ ,  $\epsilon_{\text{B}, -2} = 1$  and the luminosity distance  $d_L \simeq 10^{27.5}$  cm appropriate for GRB 030329. In both panels, we show both the limit discussed by Frail et al. (2000, dashed lines) and the deep Newtonian stage presented in this work (solid lines). Top panel: for fixed  $\epsilon_e = 0.1$ , we show the light curves for different electron power-law slopes  $p$ . The contribution of the counter-jet is artificially neglected, to show clearly that the late-time decay is in agreement with our analytical estimates (dotted lines). Bottom panel: for fixed  $p = 2.5$ , we show the light curves for different  $\epsilon_e$ , still neglecting the contribution of the counter-jet.

between the two temporal decay slopes increases. For  $p = 3$ , at the upper extreme of the range  $2 < p < 3$  where our analysis is applicable,  $F_\nu \propto t^{-1.2}$  in our model, whereas  $F_\nu \propto t^{-2.4}$  in Frail et al. (2000).

The light curves plotted in the top panel are obtained for a fixed fraction  $\epsilon_e = 0.1$  of shock energy transferred to the accelerated electrons. Yet, the power-law slope  $p$  changes, as indicated in the legend, so  $\bar{\epsilon}_e = \epsilon_e 4(p-2)/(p-1)$  is larger for higher values of  $p$ . This causes the onset of the deep Newtonian phase (as marked by the divergence between the solid and dashed lines) to occur later for larger  $p$ , in agreement with Equation (5). A more dramatic effect on the onset time  $t_{\text{DN}}$  of the deep Newtonian phase is produced by a change in the electron acceleration efficiency  $\epsilon_e$ , as shown in the bottom panel of Figure 1. As stated by Equation (5), the transition to the deep Newtonian regime happens earlier for smaller  $\epsilon_e$ . For  $\epsilon_e \lesssim 10^{-2}$ , the deep Newtonian phase promptly

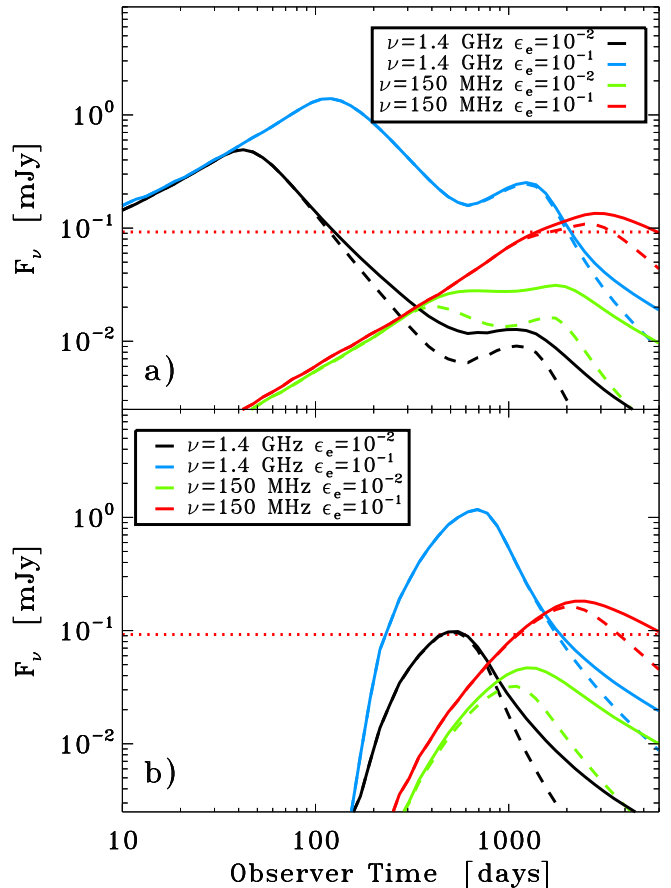


FIG. 2.— Synthetic light curves extracted from relativistic hydrodynamical simulations, for frequencies 150 MHz and 1.4 GHz and electron acceleration efficiencies  $\epsilon_e = 10^{-2}$  and  $\epsilon_e = 10^{-1}$ . We employ  $E_{51.5} = 1$ ,  $n_1 = 1$ ,  $\epsilon_{\text{B}, -2} = 1$ ,  $p = 2.5$  and the luminosity distance  $d_L \simeq 10^{27.5}$  cm appropriate for GRB 030329. In both panels, we show both the limit discussed by Frail et al. (2000, dashed lines) and the deep Newtonian stage presented in this work (solid lines). The rebrightening at late times is produced by the counter-jet. Top panel: on-axis observer ( $\theta_{\text{obs}} = 0$ ). Bottom panel: off-axis observer ( $\theta_{\text{obs}} = \pi/2$ ). In both panels, the red dotted horizontal lines show the sensitivity limit of LOFAR at 150 MHz with 24 hours of integration time.

follows the relativistic deceleration stage, and the non-relativistic phase of Frail et al. (2000) does not occur.

The effect of the electron acceleration efficiency  $\epsilon_e$  on the afterglow flux is further investigated in Figure 2, where we show the light curves obtained with our model (solid lines), and the results following Frail et al. (2000) (dashed curves). We include the contribution of the counter-jet, and we explore two values of the electron acceleration efficiency ( $\epsilon_e = 10^{-2}$  and  $\epsilon_e = 10^{-1}$ ), two observing frequencies ( $\nu = 150$  MHz and  $\nu = 1.4$  GHz), and two choices for the line of sight (on axis observer in the top panel and edge-on observer in the bottom panel).

At  $\nu = 1.4$  GHz, if the electron acceleration efficiency is small (see the black line in the top panel), the on-axis flux from the forward shock at  $t \sim 1000$  days is so bright (as compared to predictions based on Frail et al. 2000) that it might mask the contribution from the counter-jet. In fact, the counter-jet rebrightening appears much shall-

lower in our model (solid black line in the top panel) than in the prescription by Frail et al. (2000, dashed black curve). This might explain the absence of clear counter-jet signatures in the late-time radio afterglow of GRB 030329 (Mesler et al. 2012). Yet, this would require a relatively small electron acceleration efficiency ( $\epsilon_e \lesssim 0.01$ ). In fact, for the fiducial value  $\epsilon_e = 0.1$  (blue lines in the top panel), the counter-jet peak flux at  $t \sim 1000$  days does not depend on the prescription for electron acceleration. It is only at later times ( $t \gtrsim 2000$  days) that the flux approaches the predictions for the deep Newtonian phase as discussed in Equation (12), modulo an increase by a factor of two for the counter-jet contribution.

At smaller frequencies ( $\nu = 150$  MHz, green lines for  $\epsilon_e = 10^{-2}$  and red for  $\epsilon_e = 10^{-1}$ ), Figure 2 shows that even the peak of the light curve is sensitive to the prescription of electron acceleration. Our formalism (solid lines) predicts a broader peak with higher flux, as compared to the model by Frail et al. (2000) (dashed lines).<sup>8</sup> This has two important consequences. First, it will improve the chances for LOFAR detections of GRB afterglows at late times (van der Horst et al. 2008), since the peak flux for on-axis observers (red line in the top panel) approaches the sensitivity limit of LOFAR at 150 MHz (van Haarlem & al. 2013), with 24 hours of integration time (red dotted line). Second, the estimates relative to the detection at  $\sim 100$  MHz frequencies of off-axis afterglows (orphan afterglows) should be revised upwards, if the blast wave is in the deep Newtonian phase. In this stage, the peak flux for edge-on observers (red line in the bottom panel) is within the sensitivity window of LOFAR at 150 MHz.

### 3. OTHER APPLICATIONS: AFTERGLOWS FROM TDE JETS, RADIO SUPENOVAE, SLOW EJECTA FROM NEUTRON STAR MERGERS

The theory developed here for the emission from the late stages of a GRB blast wave is applicable to a number of sources with trans-relativistic ( $\beta \sim 0.1 - 0.5$ ) ejecta. Our prediction that the observed flux density will be larger than argued by previous models (e.g., Frail et al. 2000), as a result of an unavoidable change in the properties of the shock-accelerated electrons, indicates that the detectability of such sources by current and future observing facilities is better than previously thought.

The recently discovered transient jet from a supermassive black hole (Levan & al. 2011) is believed to be produced by a stellar tidal disruption event (TDE; Bloom & al. 2011; Burrows & al. 2011; Zauderer & al. 2011). The radio emission from this event is modeled as the result of the interaction between the jet and the interstellar medium, similarly to GRB afterglows (e.g., Giannios & Metzger 2011; Metzger et al. 2012; Berger et al. 2012; Zauderer et al. 2013). The radio emission remains bright even two years after the TDE (Zauderer et al. 2013) and should remain observable at  $\sim$ GHz frequencies for years to come. Given the estimates of the blast energy and surrounding density (Zauderer et al. 2013), we expect that the blast may enter the deep Newtonian regime in the next few years,

<sup>8</sup> For the green lines in the top panel, the peak at  $t \sim 500$  days is due to the self-absorption frequency passing through the observing band, whereas the bump at  $t \sim 2000$  days is produced by the contribution of the counter-jet.

making a good target to test our model.

Trans-relativistic explosions have been observationally inferred in a number of supenovae (e.g., Soderberg & al. 2008) and are theoretically predicted in double neutron star mergers (kilonovae; Li & Paczyński 1998; Metzger et al. 2010; Barnes & Kasen 2013). Electromagnetic signatures of the latter is critical in maximizing the science outputs from future gravitational wave detections (e.g., Metzger & Berger 2012). Still, previous estimates for the radio emission from such transients were rather pessimistic for the detection prospects, if the ejecta have velocity  $\beta \lesssim 0.2$  (Nakar & Piran 2011). Following our prescription for the electron distribution, the peak flux  $f_{\text{peak}}$  for ejecta with  $\beta \sim 0.1$  is typically a factor of a few higher than that calculated using the older prescription for electron acceleration (for  $\epsilon_e = 0.1$  and  $p = 2.5$ ). As a result of the increased flux, the timescale  $T$  over which the source is detectable is also prolonged. Since the detectability of a source in a magnitude-limited survey scales as  $\sim f_{\text{peak}}^{3/2} T$ , there will be a substantial increase in the detection rates.

## 4. SUMMARY AND DISCUSSION

We have described a novel evolutionary stage of GRB afterglows, when the bulk of the shock-accelerated electrons are non-relativistic, and most of the electron energy is contributed by particles with  $\gamma \sim 2$ . This phase, which we refer to as the “deep Newtonian phase,” necessarily regulates the late-time evolution of GRB afterglows, at  $t \gtrsim t_{\text{DN}} \simeq 3 \epsilon_{e,-1}^{5/6} t_{\text{ST}}$ , where  $t_{\text{ST}}$  marks the transition to the non-relativistic spherically-symmetric Sedov–Taylor solution. For typical parameters, the onset of the deep Newtonian stage occurs  $\sim 0.5$ –several years after the GRB. The deep Newtonian phase usually follows the non-relativistic regime discussed by Frail et al. (2000), which applies if the blast wave is non-relativistic, but the accelerated electrons are still ultra-relativistic. However, if the electron acceleration efficiency is  $\epsilon_e \lesssim 0.03$ , then  $t_{\text{DN}} \lesssim t_{\text{ST}}$ , i.e., the blast wave transitions from the relativistic deceleration stage directly to the deep Newtonian phase, and the non-relativistic stage presented by Frail et al. (2000) does not occur.

We now describe the observational implications of our findings. Our main focus is on GRB afterglows, but our conclusions will be relevant for other systems with trans-relativistic outflows, i.e., afterglows from tidal disruption jets, radio supenovae, and trans-relativistic ejecta from double neutron star mergers.

Radio observations at 1 – 10 GHz for  $t \gtrsim 500 - 1000$  days are available for a number of GRBs (e.g., Frail et al. 2004), most notably GRB 970508 (Waxman et al. 1998), GRB 980703 (Berger et al. 2004), and GRB 030329 (Frail et al. 2005; Mesler et al. 2012). The shallow  $\sim t^{-1}$  decline of a number of late radio afterglows (e.g., Frail et al. 2004) may indicate that the deep Newtonian phase has been already observed in several bursts (we predict that the flux in the deep Newtonian phase should indeed decay as  $F_\nu \propto t^{-(0.9 \div 1.2)} \sim t^{-1}$ ). Even more importantly, the current brightness and the fact that the flux drops as  $\sim t^{-1}$  make it possible to continue studying these afterglows for several years to come. With the full frequency coverage of the Expanded VLA (EVLA), it will be possible to cover the entire 1 – 10 GHz frequency

range in a few hours of observations, to a sensitivity that is about an order of magnitude better than that of the VLA.

In summary, current and future observational capabilities will open a new window on the late-time stages of GRB afterglows. A single radio measurement (single epoch and frequency) will probably be insufficient to determine whether the blast wave is in the deep Newtonian phase, or in the shallow Newtonian regime discussed by Frail et al. (2000). Our model predicts brighter fluxes, since  $F_\nu \propto t^{-3(p+1)/10} \propto t^{-(0.9 \div 1.2)}$  in the deep Newtonian phase (see Equation (12)), whereas  $F_\nu \propto t^{-3(5p-7)/10} \propto t^{-(0.9 \div 2.4)}$  in the regime of Frail et al. (2000) (see Equation (9)). Yet, the flux difference might be compensated by a larger value for the fitting parameter  $\epsilon_e$ . If observations at two radio frequencies are available, the radio spectral slope  $-(p-1)/2$  will constrain the electron power-law slope  $p$ , and the temporal decay of the late-time light curve will promptly distinguish between shallow and deep Newtonian regime.

Radio observations of late-time afterglows will provide an energy estimate of the explosion (e.g., Berger et al. 2004; Shivvers & Berger 2011). The calorimetric estimates in the Newtonian phase would be independent of jet collimation, since the blast wave approaches spherical symmetry. Second, this regime relies on the simple and well-understood ST dynamics of spherical blast waves. Finally, the afterglow is observable for several hundred

days in the radio band, which allows better constraints on the calorimetry. Even with a single radio measurement, one can put some constraints on the burst energy: as described by Equation (12), one fixes  $\epsilon_B, \epsilon_e$  and the only free parameters are  $n, E_j$ . In the deep Newtonian regime discussed in this work, we have the advantage that  $F_\nu \propto t^{-(0.9 \div 1.2)} \sim t^{-1}$  regardless of the uncertain slope  $p$ , whereas in the limit of Frail et al. (2000) the temporal decay depends more sensitively on  $p$ .

Finally, the deep Newtonian phase will directly impact the detection prospects at the frequencies probed by LOFAR (van der Horst et al. 2008; van Haarlem & al. 2013). For  $\sim$ GHz frequencies, the peak of the light curve happens before the deep Newtonian regime. However, as shown in Figure 2, for LOFAR frequencies ( $\sim 100 - 200$  MHz), our model for the deep Newtonian phase gives a brighter and broader peak, with respect to the prescription discussed by Frail et al. (2000). This will significantly improve the chances for LOFAR detections of GRB afterglows at late times, for both on-axis observers and edge-on observers (i.e., orphan afterglows).

L.S. is supported by NASA through Einstein Postdoctoral Fellowship grant number PF1-120090 awarded by the Chandra X-ray Center, which is operated by the Smithsonian Astrophysical Observatory for NASA under contract NAS8-03060. L.S. gratefully thanks H. J. van Eerten for help in using the Afterglow Library.

## APPENDIX

### THE CASE OF STEEP ( $p \geq 3$ ) ELECTRON DISTRIBUTIONS

The results presented in the main text assume that the distribution of accelerated electrons is in the form of a power law with slope  $2 < p < 3$ , for  $\gamma \geq \gamma_m$ . In this case, which is supported by the observations, most of the electrons (by number) are close to the minimum Lorentz factor  $\gamma_m$ , whereas the energy census is dominated by electrons with  $\gamma \sim 2$ . Here, we derive the temporal scalings expected in the deep Newtonian phase for steep electron spectra with  $p \geq 3$ , when  $\gamma_m$  dominates both in energy and particle number.

If we define the characteristic frequency  $\nu_{\text{pk}}$  as being emitted by mildly relativistic particles with  $\gamma_{\text{pk}} \sim 2$ , we have  $\nu_{\text{pk}} \propto t^{-3/5}$  as in Equation (10). Yet, we remind that for  $p \geq 3$ , mildly relativistic electrons with  $\gamma \sim 2$  do not dominate the energy balance, as opposed to the case  $2 < p < 3$  presented in the main text.

The flux emitted at the characteristic frequency  $\nu_{\text{pk}}$  needs to take into account that only a small fraction of electrons are accelerated to ultra-relativistic energies, thus contributing to the emission. If  $x_m = \gamma_m - 1 \propto \beta^2$  is the minimum of the electron distribution, then the fraction of electrons that are ultra-relativistic (i.e., with  $\gamma \gtrsim 2$ ) is  $\sim x_m^{(p-1)/2}$ . The flux at the characteristic frequency  $\nu_{\text{pk}}$  then scales as  $L_{\text{pk}} \propto BR^3 n x_m^{(p-1)/2} \propto t^{3(2-p)/5}$ . Finally, the flux at the observing frequency  $\nu$  decays in time as

$$F_\nu \propto L_{\text{pk}} (\nu_{\text{pk}}/\nu)^{(p-1)/2} \propto t^{\frac{3(5-3p)}{10}} \nu^{\frac{1-p}{2}}, \quad (\text{A1})$$

which extends the result in Equation (12) to the case  $p \geq 3$ .

### SCALINGS IN A WIND-LIKE DENSITY PROFILE

In the main body of the paper, we have assumed that the circumburst density is uniform, which is supported by recent radio observations of late-time afterglows (e.g., Mesler et al. 2012). For the sake of completeness, here we provide the expected scalings in the case that the circumburst density follows a wind-like profile,  $n = A/(m_p R^2)$ . If we define  $A = 10^{12} A_{12} \text{ g cm}^{-1}$ , the radius of the Sedov-Taylor solution evolves as

$$R \simeq 4.4 \times 10^{18} (E_{51.5}/A_{12})^{1/3} t_{10\text{yr}}^{2/3} \text{ cm}, \quad (\text{B1})$$

where  $t = 10 t_{10\text{yr}}$  years. The blast velocity in units of the speed of light is

$$\beta \simeq 0.3 (E_{51.5}/A_{12})^{1/3} t_{10\text{yr}}^{-1/3}. \quad (\text{B2})$$

The deep Newtonian phase begins when  $(\gamma_m - 1)m_e c^2 \sim m_e c^2$ , where  $\gamma_m$  is calculated from Equation (4). We find

$$t_{\text{DN}} \simeq 20 (E_{51.5}/A_{12}) \bar{\epsilon}_{e,-1}^{3/2} \text{ years}, \quad (\text{B3})$$

which is significantly longer, for standard parameters, than in the case of a uniform medium.

By assuming that a fraction  $\epsilon_B$  of the shock energy is converted into magnetic fields, the field strength will be

$$B \simeq 0.002 \epsilon_{B,-2}^{1/2} A_{12}^{1/2} t_{10\text{yr}}^{-1} \text{ G}. \quad (\text{B4})$$

When the low-energy end of the electron distribution is still ultra-relativistic (i.e., in the limit by Frail et al. 2000), the characteristic synchrotron frequency emitted by electrons with  $\gamma_{\text{pk}} \sim \gamma_m$  is

$$\nu_{\text{pk}} \sim \nu_m \simeq 5.2 \times 10^4 \bar{\epsilon}_{e,-1}^2 \epsilon_{B,-2}^{1/2} E_{51.5}^{4/3} A_{12}^{-5/6} t_{10\text{yr}}^{-7/3} \text{ Hz}, \quad (\text{B5})$$

the luminosity at the peak frequency is

$$L_{\text{pk}} \sim L_m \simeq 2.7 \times 10^{31} \epsilon_{B,-2}^{1/2} E_{51.5}^{1/3} A_{12}^{7/6} t_{10\text{yr}}^{-1/3} \text{ erg s}^{-1} \text{ Hz}^{-1}, \quad (\text{B6})$$

and the flux observed from a burst at a distance of  $d_L \simeq 10^{27.5}$  cm will be

$$\begin{aligned} F_\nu &= L_m / (4\pi d_L^2) (\nu_m / \nu)^{(p-1)/2} \\ &\simeq 0.02 \bar{\epsilon}_{e,-1}^{p-1} \epsilon_{B,-2}^{\frac{1+p}{4}} E_{51.5}^{\frac{4p-3}{3}} A_{12}^{\frac{19-5p}{12}} t_{10\text{yr}}^{\frac{5-7p}{6}} \nu_{\text{GHz}}^{\frac{1-p}{2}} d_{27.5}^{-2} \text{ mJy}, \end{aligned} \quad (\text{B7})$$

which is in agreement with the results by Livio & Waxman (2000).

Different scalings are expected in the deep Newtonian phase. Under the assumption that the electron power-law slope is  $2 < p < 3$ , the peak frequency is emitted by mildly relativistic electrons with  $\gamma_{\text{pk}} \sim 2$ , so

$$\nu_{\text{pk}} \simeq 2.4 \times 10^4 \epsilon_{B,-2}^{1/2} A_{12}^{1/2} t_{10\text{yr}}^{-1} \text{ Hz}, \quad (\text{B8})$$

the peak luminosity scales in time as  $L_{\text{pk}} \propto t^{-1}$ , and the flux at frequency  $\nu$  decays as

$$\begin{aligned} F_\nu &= L_{\text{pk}} / (4\pi d_L^2) (\nu_{\text{pk}} / \nu)^{(p-1)/2} \\ &\simeq 0.015 \bar{\epsilon}_{e,-1} \epsilon_{B,-2}^{\frac{1+p}{4}} E_{51.5} A_{12}^{\frac{p+1}{4}} t_{10\text{yr}}^{\frac{-(1+p)}{2}} \nu_{\text{GHz}}^{\frac{1-p}{2}} d_{27.5}^{-2} \text{ mJy}, \end{aligned} \quad (\text{B9})$$

where the numerical factor has been calibrated such that it matches the flux in Equation (B7) at the onset of the deep Newtonian phase.

#### SYNCHROTRON SELF-ABSORPTION

The results presented so far implicitly assume that the self-absorption frequency lies below the observing frequency during the deep Newtonian phase. However, for observations at  $\sim 100$  MHz, the self-absorption frequency will sweep across the observing band at late times, during the deep Newtonian regime. We now derive the temporal evolution of the self-absorption frequency, for a constant density medium and a wind-like profile. As in the main body of the paper, we assume that the electron power-law slope is in the range  $2 < p < 3$ .

The self-absorption frequency  $\nu_a$  is such that the optical depth  $\tau_\nu(\nu_a) \sim \alpha_\nu R \sim 1$ , where the absorption coefficient is

$$\alpha_\nu(\nu_a) \propto \frac{\epsilon_e e_{th} B}{\gamma_{\text{pk}} \nu_a^2} \left( \frac{\nu_a}{\nu_{\text{pk}}} \right)^{-p/2}, \quad (\text{C1})$$

which is appropriate if  $\nu_a \gg \nu_{\text{pk}}$ . In the expression above,  $\gamma_{\text{pk}} \sim 2$ ,  $e_{th} \propto n\beta^2$  and  $B \propto \sqrt{\epsilon_B n} \beta$ , where  $\beta$  is the flow velocity. We now differentiate between a constant density medium and a wind-like profile.

If the circumburst density is uniform, then  $R \propto t^{2/5}$ ,  $\beta \propto t^{-3/5}$ ,  $n \propto t^0$  and the peak frequency  $\nu_{\text{pk}} \propto t^{-3/5}$  (see Equation (10)), so we obtain that the self-absorption frequency scales as

$$\nu_a \propto t^{-\frac{3p+14}{5(p+4)}} \quad [\text{uniform medium}] \quad (\text{C2})$$

For a wind-like profile, we have that  $R \propto t^{2/3}$ ,  $\beta \propto t^{-1/3}$ ,  $n \propto t^{-4/3}$  and the peak frequency  $\nu_{\text{pk}} \propto t^{-1}$  (see Appendix B), so that the self-absorption frequency scales as

$$\nu_a \propto t^{-\frac{3p+14}{3(p+4)}} \quad [\text{wind}] \quad (\text{C3})$$

In both cases, we point out that the self-absorption frequency drops faster than  $\nu_{\text{pk}}$ .

#### REFERENCES

- Berger, E., Kulkarni, S. R., & Frail, D. A. 2004, *ApJ*, 612, 966
- Berger, E., Zauderer, A., Pooley, G. G., Soderberg, A. M., Sari, R., Brunthaler, A., & Bietenholz, M. F. 2012, *ApJ*, 748, 36
- Blandford, R. & Eichler, D. 1987, *Phys. Rep.*, 154, 1
- Blandford, R. D. & Ostriker, J. P. 1978, *ApJ*, 221, L29
- Bloom, J. S. & al. 2011, *Science*, 333, 203
- Burrows, D. N. & al. 2011, *Nature*, 476, 421
- Frail, D. A., Metzger, B. D., Berger, E., Kulkarni, S. R., & Yost, S. A. 2004, *ApJ*, 600, 828
- Frail, D. A., Soderberg, A. M., Kulkarni, S. R., Berger, E., Yost, S., Fox, D. W., & Harrison, F. A. 2005, *ApJ*, 619, 994
- Frail, D. A., Waxman, E., & Kulkarni, S. R. 2000, *ApJ*, 537, 191
- Giannios, D. & Metzger, B. D. 2011, *MNRAS*, 416, 2102
- Granot, J. & Sari, R. 2002, *ApJ*, 568, 820
- Keshet, U. & Waxman, E. 2005, *Physical Review Letters*, 94, 111102
- Kirk, J. G., Guthmann, A. W., Gallant, Y. A., & Achterberg, A. 2000, *ApJ*, 542, 235
- Kumar, P. & Barniol Duran, R. 2009, *MNRAS*, 400, L75
- Levan, A. J. & al. 2011, *Science*, 333, 199
- Li, L.-X. & Paczyński, B. 1998, *ApJ*, 507, L59
- Livio, M. & Waxman, E. 2000, *ApJ*, 538, 187
- Mesler, R. A., Pihlström, Y. M., Taylor, G. B., & Granot, J. 2012, *ApJ*, 759, 4
- Metzger, B. D. & Berger, E. 2012, *ApJ*, 746, 48
- Metzger, B. D., Giannios, D., & Mimica, P. 2012, *MNRAS*, 420, 3528
- Metzger, B. D., Martínez-Pinedo, G., Darbha, S., Quataert, E., Arcones, A., Kasen, D., Thomas, R., Nugent, P., Panov, I. V., & Zinner, N. T. 2010, *MNRAS*, 406, 2650
- Nakar, E. & Piran, T. 2011, *Nature*, 478, 82
- Panaitescu, A. & Kumar, P. 2000, *ApJ*, 543, 66
- Piran, T. 2004, *Reviews of Modern Physics*, 76, 1143
- Rhoads, J. E. 1999, *ApJ*, 525, 737
- Sari, R., Piran, T., & Halpern, J. P. 1999, *ApJ*, 519, L17
- Sari, R., Piran, T., & Narayan, R. 1998, *ApJ*, 497, L17
- Shivvers, I. & Berger, E. 2011, *ApJ*, 734, 58
- Soderberg, A. M. & al. 2008, *Nature*, 453, 469
- van der Horst, A. J., Kamble, A., Resmi, L., Wijers, R. A. M. J., Bhattacharya, D., Scheers, B., Rol, E., Strom, R., Kouveliotou, C., Oosterloo, T., & Ishwara-Chandra, C. H. 2008, *A&A*, 480, 35
- van Eerten, H., van der Horst, A., & MacFadyen, A. 2012, *ApJ*, 749, 44
- van Eerten, H., Zhang, W., & MacFadyen, A. 2010a, *ApJ*, 722, 235
- van Eerten, H. J., Leventis, K., Meliani, Z., Wijers, R. A. M. J., & Keppens, R. 2010b, *MNRAS*, 403, 300
- van Eerten, H. J. & MacFadyen, A. I. 2011, *ApJ*, 733, L37
- . 2012, *ApJ*, 751, 155
- van Eerten, H. J. & Wijers, R. A. M. J. 2009, *MNRAS*, 394, 2164
- van Haarlem, M. P. & al. 2013, *ArXiv/astro-ph:1305.3550*
- Waxman, E., Kulkarni, S. R., & Frail, D. A. 1998, *ApJ*, 497, 288
- Wijers, R. A. M. J. & Galama, T. J. 1999, *ApJ*, 523, 177
- Wygoda, N., Waxman, E., & Frail, D. A. 2011, *ApJ*, 738, L23
- Zauderer, B. A. & al. 2011, *Nature*, 476, 425
- Zauderer, B. A., Berger, E., Margutti, R., Pooley, G. G., Sari, R., Soderberg, A. M., Brunthaler, A., & Bietenholz, M. F. 2013, *ApJ*, 767, 152
- Zhang, W. & MacFadyen, A. 2009, *ApJ*, 698, 1261